Macromolecules

ARTICLE

pubs.acs.org/Macromolecules

Thermal Stability of Poly[2-methoxy-5-(2′-phenylethoxy)-1,4-phenylenevinylene] (MPE-PPV):Fullerene Bulk Heterojunction Solar Cells

J. Vandenbergh,[†] B. Conings,[†] S. Bertho,[†] J. Kesters,[†] D. Spoltore,[†] S. Esiner,[‡] J. Zhao,[§] G. Van Assche,[§] M. M. Wienk,[‡] W. Maes,[†,∥] L. Lutsen,[⊥] B. Van Mele,[§] R. A. J. Janssen,[‡] J. Manca,[†,⊥] and D. J. M. Vanderzande*[,†,⊥]

[†]Institute for Materials Research (IMO), Hasselt University, Universitaire Campus, Building D, B-3590 Diepenbeek, Belgium

[‡]Molecular Materials and Nanosystems, Eindhoven University of Technology, P.O. Box 513, 5600MB Eindhoven, The Netherlands

[§]Physical Chemistry and Polymer Science, Department of Materials and Chemistry, Vrije Universiteit Brussel, Pleinlaan 2, B-1050 Brussels, Belgium

[∥]Molecular Design and Synthesis, Katholieke Universiteit Leuven, Celestijnenlaan 200F, B-3001 Heverlee, Belgium

[⊥]Division IMOMEC, IMEC, Universitaire Campus, Wetenschapspark 1, B-3590 Diepenbeek, Belgium

Supporting Information

ABSTRACT: To improve the thermal stability of polymer:fullerene bulk heterojunction solar cells, a new polymer, poly[2-methoxy-5-(2′-phenylethoxy)-1,4-phenylenevinylene] (MPE-PPV), has been designed and synthesized, which showed an increased glass transition temperature (T_g) of 111 °C. The thermal characteristics and phase behavior of MPE-PPV:[6,6]-phenyl C_{61}-butyric acid methyl ester ([60]PCBM) blends were investigated by means of modulated temperature differential scanning calorimetry and rapid heating−cooling calorimetry. The thermal stability of MPE-PPV:[60]PCBM solar cells was compared with devices based on the reference MDMO-PPV material with a T_g of 45 °C. Monitoring of the photocurrent−voltage characteristics at elevated temperatures revealed that the use of high-T_g MPE-PPV resulted in a substantial improvement of the thermal stability of the solar cells. Furthermore, a systematic transmission electron microscope study of the active polymer:fullerene layer at elevated temperatures likewise demonstrated a more stable morphology for the MPE-PPV:[60]PCBM blend. Both observations indicate that the use of high-T_g MPE-PPV as donor material leads to a reduced free movement of the fullerene molecules within the active layer of the photovoltaic device. Finally, optimization of the PPV:fullerene solar cells revealed that for both types of devices the use of [6,6]-phenyl C_{71}-butyric acid methyl ester ([70]PCBM) resulted in a substantial increase of current density and power conversion efficiency, up to 3.0% for MDMO-PPV:[70]PCBM and 2.3% for MPE-PPV:[70]PCBM.

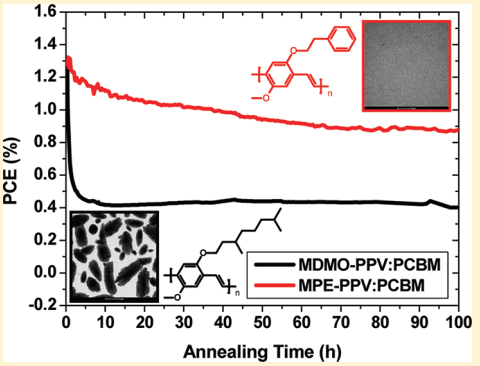

INTRODUCTION

In polymer:fullerene bulk heterojunction solar cells, the nanoscale morphology of the active layer influences the electronic properties of the devices to a great extent.[1−4] Via proper sample preparation, such as annealing conditions and the choice of processing solvents, the (nano)morphology of the donor−acceptor blend can be optimized, leading to improved exciton dissociation and charge transport.[3−6] It was already demonstrated, however, that this initial optimized morphology deteriorates rather fast (during storage at elevated temperatures).[7−17] Long-term annealing treatments induce severe phase separation between the donor polymer and the fullerene acceptor material, leading to a decreased interfacial area and less efficient exciton dissociation.[18−20] To stabilize the initial (nano)morphology of a bulk heterojunction layer, several pathways can be followed. A first approach is to use donor−acceptor diblock copolymers to covalently fixate the morphology via the scale of the block lengths.[13,14] A second way to obtain a stable network is to build in a certain amount of functional groups in the donor polymer which can cross-link and freeze in the ultimate morphology after a thermal or UV light treatment.[21] In this paper, a third approach is further investigated, which is based on the use of a donor polymer with a high glass transition temperature (T_g).[22−26] In this context the question arises how to adjust the chemical structure of the polymer to induce a higher T_g, without jeopardizing the optoelectronic characteristics of the polymer. Here we demonstrate that by changing the side-chain substituents of the polymer, the T_g can be deliberately increased. Poly[(2-methoxy-5-(3′,7′-dimethyloctyloxy))-1,4-phenylenevinylene] (MDMO-PPV) has a quite low T_g of around 45 °C due to the long flexible alkoxy side chains, which cause a plasticizing effect on the PPV backbone.[22] To reduce the side-chain flexibility, a novel poly(*p*-phenylenevinylene) derivative, poly[2-methoxy-5-(2′-phenylethoxy)-1,4-phenylenevinylene]

Received: August 22, 2011
Revised: October 2, 2011
Published: October 17, 2011

(MPE-PPV), has been designed and synthesized. The bulky and rigid phenyl side groups decrease the rotational freedom of the polymer backbone, thereby increasing the T_g at which the amorphous polymer transfers from a rigid glass into soft flexible material. The T_g of the polymer as well as the phase behavior in blends with [6,6]-phenyl C_{61}-butyric acid methyl ester ([60]PCBM) was determined by means of advanced thermal analysis techniques, i.e., modulated temperature differential scanning calorimetry (MTDSC) and rapid heating−cooling calorimetry (RHC). The effect of elevated temperatures on the bulk morphology of MPE-PPV:[60]PCBM blends and the photovoltaic performance of the resulting devices was studied via transmission electron microscopy (TEM) and via in-situ monitoring of the photovoltaic output (i.e., the short circuit current, open circuit voltage, fill factor, and efficiency). The results will be compared with reference MDMO-PPV:[60]PCBM solar cells. Finally, the MPE-PPV:fullerene and MDMO-PPV:fullerene devices were optimized for maximal photovoltaic output. Different spin-coating solvents were applied, and both [60]PCBM and [6,6]-phenyl C_{71}-butyric acid methyl ester ([70]PCBM) fullerene derivatives were used as acceptor materials.

EXPERIMENTAL SECTION

General. Unless stated otherwise, all reagents and chemicals were obtained from commercial sources (Acros and Aldrich) and used without further purification. 1,4-Dioxane was dried by distillation from Na/benzophenone. NMR spectra were recorded with a Varian Inova 300 spectrometer using a 5 mm probe. Gas chromatography/mass spectrometry (GC/MS) analyses were carried out with TSQ-70 and Voyager mass spectrometers (Thermoquest); the capillary column was a Chrompack Cpsil5CB or Cpsil8CB. Analytical size exclusion chromatography (SEC) was performed using a Spectra series P100 (Spectra-Physics) pump equipped with two mixed-B columns (10 μm, 0.75 cm × 30 cm, Polymer Laboratories) and a refractive index detector (Shodex) at 40 °C. THF was used as the eluent at a flow rate of 1.0 mL/min. Molecular weight distributions are given relative to polystyrene standards. FT-IR spectra were collected with a Perkin-Elmer Spectrum One FT-IR spectrometer (nominal resolution 4 cm^{-1}, summation of 16 scans). UV−vis spectroscopy was performed on a Varian Cary 500 UV−vis−NIR spectrophotometer (scan rate 600 nm/min). Samples for thin-film FT-IR and UV−vis characterization were prepared by drop-casting the precursor polymer from a $CHCl_3$ solution (10 mg/mL) onto NaCl or quartz disks.

The DSC and MTDSC measurements were performed on a TA Instruments Q2000 DSC (Tzero DSC technique) with the MDSC option, equipped with an RCS cooling accessory and purged with nitrogen (50 mL min^{-1}). Baseline, heat capacity, and temperature were calibrated with sapphire and indium. About 5 mg samples were sealed in aluminum crucibles (Tzero, 40 μL). For the DSC measurements, the samples were heated and cooled between −90 and 300 °C at 10 K min^{-1}. To reduce the sample preparation effects, the first cooling and the second heating were used for discussion. Actually, such a methodology can to a certain extent avoid the effects of casting solvents[19,20] and annealing conditions.[6,21] Heating and cooling curves of subsequent cycles coincide. The melting and crystallization peaks were characterized by their peak temperatures. For the MTDSC measurements, the modulation amplitude was 0.5 K with a period of 60 s. First, the samples were kept at 300 °C for 1 min. Subsequently, they were quenched in the DSC cell at about 100 K min^{-1} to −90 °C and then reheated to 300 °C at 2.5 K min^{-1}. The RHC measurements were performed on a TA Instruments RHC prototype (Tzero DSC technique) equipped with a LNCS cooling accessory and purged with neon (10 mL min^{-1}). Baseline, heat capacity, and temperature were calibrated with sapphire and indium. About 0.5 mg samples were sealed in aluminum RHC crucibles with a weight of less than 2 mg. First, the samples were heated to 350 °C for 0.1 min. Subsequently, they were quenched in the RHC cell to −150 °C and then reheated to 350 °C at 500 K min^{-1}.

Nonoptimized bulk heterojunction solar cells, combining either poly[(2-methoxy-5-(3′,7′-dimethyloctyloxy))-1,4-phenylenevinylene] (MDMO-PPV) with $T_g \approx 45$ °C (Covion, $M_w = 716$ kg/mol, PD = 6.5) or poly[(2-methoxy-5-(2′-phenylethoxy))-1,4-phenylenevinylene] (MPE-PPV) with $T_g \approx 111$ °C ($M_w = 123$ kg/mol, PD = 2.3), as electron donor materials with [60]PCBM (Solenne-BV) as acceptor material were made according to the following preparation guidelines. The devices had an ITO/PEDOT−PSS/polymer:[60]PCBM/Ca/Al structure. Each device had an active area of 25.0 mm^2. Indium tin oxide (ITO, 100 nm)-coated glass plates were successively cleaned in a soap solution, demineralized water, and acetone, each for 10 min in an ultrasonic bath. This was followed by an additional cleaning step in boiling isopropanol for 10 min and an UV/O_3 treatment of 30 min. A 60 nm thick poly(3,4-ethylenedioxythiophene−polystyrenesulfonate (PEDOT−PSS (HC Starck, Clevios P VP AI 4083)) layer was spin-coated on the clean glass/ITO substrates. The substrates were dried for 20 min on a hot plate at 120 °C. The active layer, with thickness of 80 nm, consisting of a blend of the respective PPV polymer and [60]PCBM in chlorobenzene, was spin-coated on top of the PEDOT−PSS layer. The polymer:[60]PCBM ratio for MDMO-PPV and MPE-PPV was 1:4 (this ratio was chosen because it resulted in the best solar cell performance). The concentrations of the polymer solutions were 0.5 wt % (weight percentage of polymer in chlorobenzene solvent). To obtain complete dissolution, the polymer:[60]PCBM solutions were stirred overnight at 50 °C. The solar cells were completed by subsequently evaporating 20 nm of Ca on top of the active layer, followed by 60 nm of Al. The current−voltage (*IV*) characteristics were measured with a Newport class A solar simulator (model 91195A) calibrated with a silicon solar cell to give an AM1.5 spectrum. The influence of thermal annealing on the photovoltaic performance was measured in a setup that measures *IV* characteristics at regular time intervals (illumination with a White LED LZ4-00CW10 (LedEngin)) while the samples were kept under continuous annealing in a nitrogen atmosphere. In between the measurements, the samples were kept in the dark. The active layer morphology was studied with a transmission electron microscope (FEI Tecnai Spirit), operated at 120 kV. To prepare TEM specimens, the flotation technique was used to remove the films from the glass surface via treatment with HF (40%). The films floating on the surface of deionized water were subsequently picked up by a 400 mesh copper grid.

Optimized bulk heterojunction solar cells with either MDMO-PPV or MPE-PPV as electron donor materials and either [60]PCBM or [70]PCBM (Solenne-BV) as acceptor material were made according to the following preparation guidelines. The devices had an ITO/PEDOT−PSS/polymer:fullerene/LiF/Al structure. The devices had active areas of either 9 or 16 mm^2. Indium tin oxide (ITO, 100 nm)-coated glass plates were successively cleaned and rubbed in acetone, ethanol, soap solution, demineralized water, and isopropanol, each for 15 min in an ultrasonic bath, followed by an UV/O_3 treatment of 30 min. A 60 nm thick PEDOT-PSS (HC Starck, Clevios P VP AI 4083) layer was spin-coated on the clean glass/ITO substrates. Subsequently, polymer:fullerene (1:4) active layers with different thicknesses were spin-coated from different solvents on top of the PEDOT-PSS layer. The concentrations of the solutions were 0.5 wt % (weight percentage of polymer in solvent) for both polymers. To obtain complete dissolution, the polymer:fullerene solutions were stirred overnight at 60 °C. The toluene solutions were stirred subsequently at 90 °C for 1 h. The solar cells were completed by subsequently evaporating 1 nm of LiF on top of the active layer, followed by 100 nm of Al. The current−voltage (*IV*) characteristics were measured with a Keithley 2400 SMU, under white light illumination with UV(GG 385) and infrared (KG1) filtered light

Scheme 1. Synthesis of MPE-PPV via the Gilch Precursor Route[a]

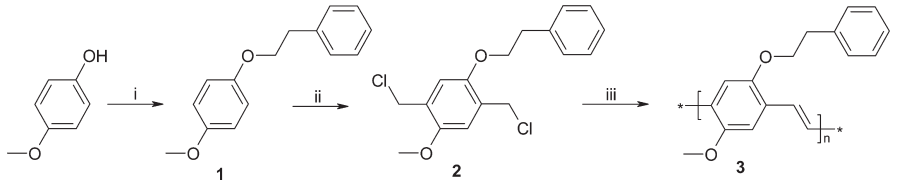

[a] Reagents and conditions: (i) 2-bromoethylbenzene, Na*t*BuO, NaI, EtOH (39% yield); (ii) *p*-CH_2O, Ac_2O, HCl (88% yield); (iii) 1: K*t*BuO, 1,4-dioxane; 2: ΔT (56% yield).

from a tungsten halogen lamp with a maximum estimated light output of 1000 W/m^2. The solar simulator was calibrated with a silicon solar reference cell. The currents reported were corrected for spectral mismatch.[8]

Synthesis. 1-Methoxy-4-(2′-phenylethoxy)benzene (1). In a three-necked round-bottom flask, 4-methoxyphenol (32.0 g, 0.256 mol) and Na*t*BuO (29.8 g, 0.310 mol) were dissolved in ethanol (260 mL). The mixture was stirred for 1 h at ambient temperature under a nitrogen atmosphere. Subsequently, 2-bromoethylbenzene (52.1 g, 0.280 mol) was added dropwise to the mixture, and NaI (1.0 g, 0.007 mol) was additionally added in one go. The mixture was heated at reflux for 16 h under a nitrogen atmosphere. Water (200 mL) was added, ethanol was evaporated, and the mixture was extracted with $CHCl_3$ (3 × 50 mL). The organic phase was washed with 10% NaOH and subsequently dried over $MgSO_4$. After filtration and evaporation of the solvent, the crude product was obtained as a clear brown solid. The product was purified by column chromatography (SiO_2, eluent hexane/chloroform 1/1) to afford white crystals. Yield: 39% (23.0 g). ^{1}H NMR ($CDCl_3$): 7.35−7.18 (m, 5H, ArH), 6.82 (s, 4H, ArH), 4.10 (t, 2H, OCH_2, J = 6.1 Hz), 3.75 (s, 3H, OCH_3), 3.07 (t, 2H, CH_2−Ar, J = 5.9 Hz). ^{13}C NMR ($CDCl_3$): 151.7, 150.8, 138.1, 129.3, 128.5, 115.0, 114.1, 69.2, 56.0, 35.7. MS (EI, m/z): 228 [M$^+$]. IR (NaCl, cm^{-1}): 2956, 2924, 2850, 1591, 1500, 1462, 1412, 1380, 1315, 1261, 1206, 1040, 867.

2,5-Bis(chloromethyl)-1-methoxy-4-(2′-phenylethoxy)benzene (2). 1-Methoxy-4-(2′-phenylethoxy)benzene (**1**) (3.2 g, 0.014 mol) and *p*-formaldehyde (1.2 g, 0.038 mol) were added to a three-necked round-bottom flask, which was placed in an ice bath and under a nitrogen atmosphere. After addition of HCl (37%) (9.0 g, 0.092 mol), acetic anhydride (14.2 g, 0.140 mol) was added dropwise at such a rate that the temperature of the mixture did not exceed 70 °C. Subsequently, the mixture was stirred for 6 h at 70 °C under a nitrogen atmosphere. Afterward, the mixture was cooled down to room temperature and decanted into water (100 mL) to form a white precipitate. After filtration of the mixture, the crude product was purified via recrystallization in $CHCl_3$ to obtain white crystals. Yield: 88% (4.0 g). ^{1}H NMR ($CDCl_3$): 7.38−7.18 (m, 5H, ArH), 6.88 (s, 2H, ArH), 4.60 (s, 2H, CH_2Cl), 4.58 (s, 2H, CH_2Cl), 4.20 (t, 2H, OCH_2, J = 6.6 Hz), 3.82 (s, 3H, OCH_3), 3.10 (t, 2H, CH_2−Ar, J = 6.4 Hz). ^{13}C NMR ($CDCl_3$): 151.2, 150.30, 138.0, 129.3, 128.5, 127.5, 127.0, 126.5, 114.5, 113.0, 69.5, 56.2, 41.0, 35.8. MS (EI, m/z): 324 [M$^+$]. IR (NaCl, cm^{-1}): 2956, 2924, 2850, 1591, 1500, 1462, 1412, 1380, 1315, 1261, 1206, 1040, 867, 736, 704, 681.

Poly[(2-methoxy-5-(2′-phenylethoxy))-1,4-phenyleneviny-lene] (MPE-PPV) (3). In a typical Gilch procedure, 2,5-bis(chloromethyl)-1-methoxy-4-(2′-phenylethoxy)benzene (**2**) (0.5 g, 1.5 mmol) was dissolved in dry 1,4-dioxane (152 mL), giving a concentration of 0.01 M. The mixture was stirred at 25 °C under a continuous flow of nitrogen. A K*t*BuO solution (1.5 equiv, 0.87 M in 1,4-dioxane) was added dropwise over a time period of 15 min to the stirred monomer solution. The reaction was kept for 2 h at 25 °C under a nitrogen atmosphere, and the mixture was subsequently quenched in ice water (100 mL). The excess of base was neutralized with HCl (1 M in H_2O). The aqueous phase was extracted with $CHCl_3$ (3 × 40 mL). After combination of the organic phases, the solvent was evaporated and the

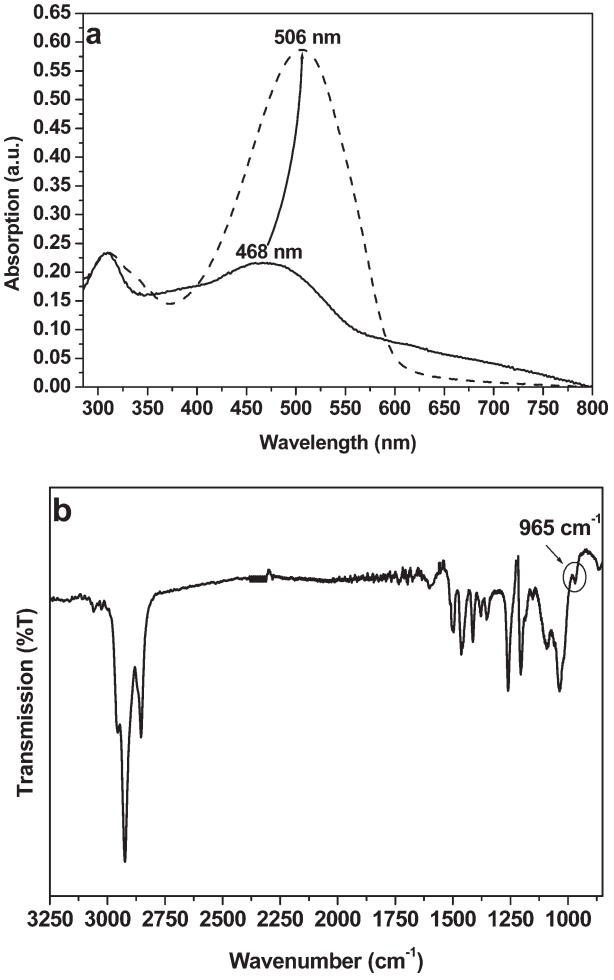

Figure 1. Thin film UV−vis spectra before (full line) and after (dashed line) thermal elimination (a) and FT-IR spectrum (b) of MPE-PPV.

polymer was redissolved in 1,4-dioxane (100 mL). The mixture was refluxed for 16 h under a nitrogen atmosphere to ensure complete formation of the conjugated system. Subsequently, the mixture was cooled down to room temperature, and the polymer was precipitated via addition of cold methanol (100 mL). The mixture was filtered, and the red fibrous polymer was collected and dried in vacuo. The residual fractions contained only monomers and oligomers. Yield: 56% (218 mg). ^{1}H NMR ($CDCl_3$): 7.6−7.0 (br, 9H, ArH/CH=CH), 4.4−4.2 (br, 2H, OCH_2), 4.0−3.8 (br, 3H, OCH_3), 3.25−2.95 (br, 2H, CH_2−Ar). ^{13}C NMR ($CDCl_3$): 151.5, 150.8, 138.2, 129.0, 128.5, 127.4, 127.0, 126.5, 123.5, 110.5, 109.1, 70.0, 56.1, 35.7. IR (NaCl, cm^{-1}): 2956, 2924, 2850, 1591, 1500, 1462, 1412, 1351, 1261, 1206, 1040, 965, 867. UV−vis (thin film): λ_{max} = 506 nm. SEC (THF): M_w = 123 × 10^3 g/mol (PD = 2.5).

dx.doi.org/10.1021/ma201911a |*Macromolecules* 2011, 44, 8470–8478

RESULTS AND DISCUSSION

Synthesis and Standard Characterization. PPV derivatives are usually prepared via precursor routes, of which the Gilch procedure (dehydrohalogenation polymerization) is the most straightforward method.[27] The desired MPE-PPV polymer was prepared through a convenient three-step sequence (Scheme 1). First, 1-methoxy-4-(2′-phenylethoxy)benzene (**1**) was synthesized using a Williamson ether reaction combining 4-methoxyphenol and 2-bromoethylbenzene. In a second step, the MPE Gilch precursor monomer, bischloromethyl derivative **2**, was prepared via chloromethylation with *p*-formaldehyde and HCl in acetic anhydride. Premonomer **2** was efficiently purified via recrystallization in chloroform.

Polymerization was performed under a nitrogen atmosphere. To this end, bis(chloromethyl) premonomer **2** was dissolved in dry 1,4-dioxane (0.01 M), after which 1.5 equiv of K*t*BuO base was added. After work-up, the orange sticky precursor polymer was isolated via precipitation in cold methanol. The precursor polymer was already partially conjugated at this stage due to the small excess of base applied during polymerization. UV−vis spectroscopy of the precursor polymer revealed an absorption maximum of 468 nm (Figure 1a). The material was converted further into a fully conjugated polymer via thermal elimination at 100 °C in 1,4-dioxane. Upon heating, the chlorine groups were eliminated to form fully conjugated MPE-PPV **3**. After work-up of the elimination reaction, the final polymer was isolated via precipitation in cold methanol. Molecular weights were determined by size exclusion chromatography (SEC). The obtained MPE-PPV had a M_w of 123 × 10^3 g/mol and a PD of 2.5. In the UV−vis spectrum, the absorption band at 468 nm shifted to 506 nm and increased in absorptivity, indicating that a fully conjugated system had developed. FT-IR spectroscopy revealed the characteristic vibration frequencies of MPE-PPV (Figure 1b). The signal at 965 cm^{-1} originates from the *trans*-vinylene double bonds of the conjugated polymer and is applied as a standard criterion for the development of the conjugated PPV system.

Thermal Analysis. The thermal properties and phase behavior of MPE-PPV:[60]PCBM blends were investigated by means of MTDSC and RHC, which is a useful tool to investigate the glass transition of semicrystalline samples due to its high scan rate (up to 2000 K min^{-1}). Both techniques were used to investigate crystallization, melting, and glass transition of the PPV:fullerene blends, with an emphasis on the different component miscibilities and possible phase separation. Differences in extent of phase separation can account for possible deviating performances of the corresponding polymer solar cells made from these blends.

In general, the initial morphology of deposited blend films is the result of a kinetically frozen phase separation or crystallization during solvent evaporation. Consequently, both thermodynamic and kinetic parameters are responsible for the morphology obtained.[28−30] The phase behavior of such blends with a well-defined thermal history is important to understand and (ultimately) control morphology development, long-term stability of the film morphology, and the photovoltaic performance of the corresponding solar cells.[31−33]

Figure 2a shows MTDSC apparent specific heat capacity (c_p^{app}) curves of MPE-PPV:[60]PCBM blends over the full composition range. From these curves, the crystallization and melting behavior of these blends can be seen. The pure MPE-PPV sample is amorphous; neither crystallization nor melting can be seen. Pure [60]PCBM samples are semicrystalline, as reported before.[33]

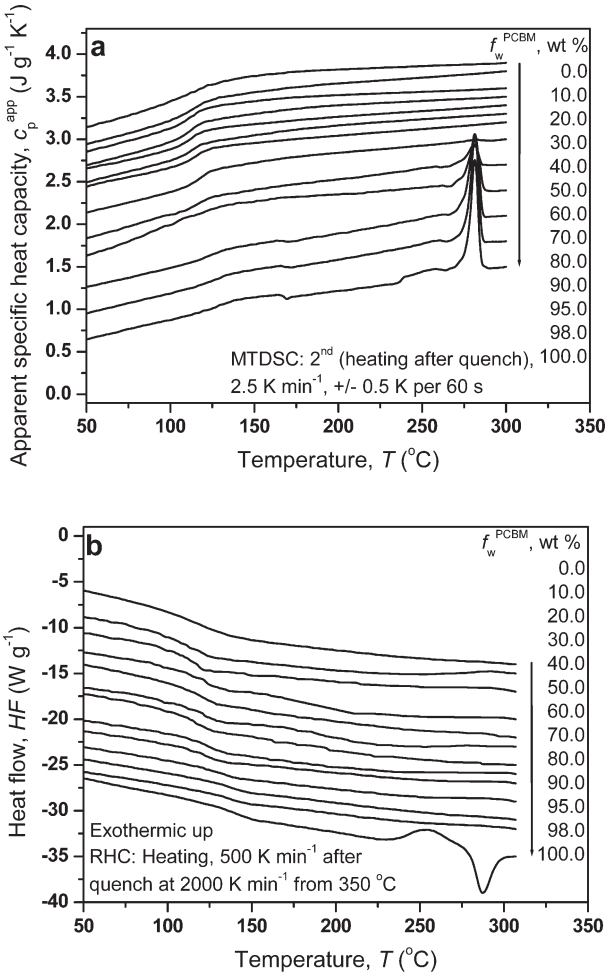

Figure 2. MTDSC thermograms showing apparent specific heat capacity (c_p^{app}) (a) and RHC thermograms showing heat flow (HF) (b) during heating after quenching for MPE-PPV:[60]PCBM blends with various $f_w^{[60]PCBM}$. All curves are shifted vertically for clarity.

Therefore, both the crystallization and melting in the blends can be attributed to the fullerene component rather than the MPE-PPV polymer. All samples were quenched at about 100 K min^{-1} to reduce the crystallinity and enhance the visibility of the glass transition. Although the crystallinity only decreased slightly due to the high crystallization rate of [60]PCBM, clear glass transitions could be seen for all the blends and pure components.

To study if phase separation occurred in MPE-PPV:[60]PCBM blends, RHC was used to study the glass transitions.[34,35] Figure 2b shows the RHC heat flow (HF) curves for the blends. It can clearly be seen that RHC can completely avoid crystallization of the PPV:[60]PCBM blends due to its considerably enhanced cooling rate, reaching a maximum of about 2000 K min^{-1}, compared to regular DSC (about 100 K min^{-1} without the use of liquid nitrogen). No melting peaks can be distinguished for the MPE-PPV:[60]PCBM blends, not even with high weight fractions of [60]PCBM ($f_w^{[60]PCBM}$), except for pure PCBM, where the melting of crystals formed during heating is observed.

Figure 3 summarizes the characteristic temperatures, melt crystallization temperature (T_{mc}), cold crystallization temperature (T_{cc}), melting temperature (T_m), and glass transition temperature (T_g), as a function of $f_w^{[60]PCBM}$. It can be observed that with decreasing $f_w^{[60]PCBM}$ the crystallization of [60]PCBM slows down

(T_{mc} increases and T_{cc} decreases slightly) and less [60]PCBM crystallizes (the melting peak area decreases). Below 70 wt % of [60]PCBM, the samples do not show crystallization or melting at the cooling and heating rates employed. With decreasing $f_w^{[60]PCBM}$, the T_g decreases gradually from the T_g of pure [60]PCBM (about 131.2 °C) to the nearly as high T_g of neat MPE-PPV (about 111.2 °C). All blends show a single T_g in between of those of the pure components.

In previous studies, it was demonstrated that MDMO-PPV:[60]PCBM blends show a clear double T_g, which is an obvious indication of phase separation in the molten state.[19,29,36] For [60]PCBM contents from 70% to 90% double glass transitions were noted, with temperatures corresponding to phases with estimated compositions of 55 ± 5% and 97 ± 2%, respectively. For the MPE-PPV:[60]PCBM blends, it was also supposed that phase separation might occur in the molten state due to the similar molecular structures. However, single T_g's were observed in our MTDSC and RHC experiments, which would indicate the absence of phase separation in the molten state. Nevertheless, due to the very close T_g's of MPE-PPV and [60]PCBM, the gap between them is only ~20 °C; it would be difficult to see two glass transition steps of partially phase-separated phases, especially since one T_g transition can be as wide as 50 °C. As shown later in this paper, TEM images show the absence of a nanoscale structure in the as-cast MPE-PPV:[60]PCBM blends, in contrast to the nanoscale structure of as cast MDMO-PPV:[60]PCBM.

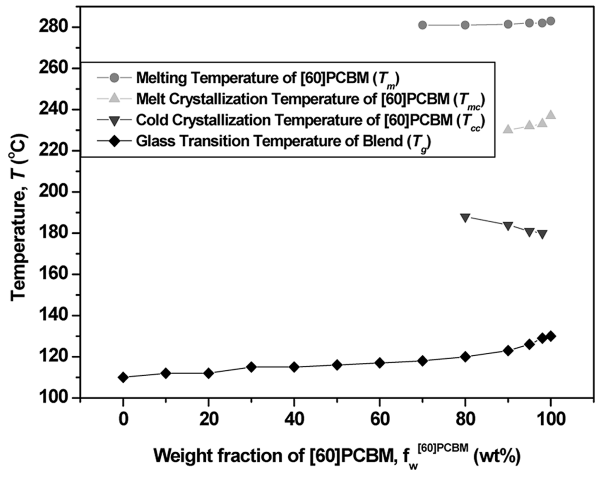

Figure 3. Dependence of the characteristic temperatures T_{mc}, T_{cc}, T_m, and T_g, measured by (MT)DSC, on the $f_w^{[60]PCBM}$ for MPE-PPV:[60]PCBM blends.

Device Characterization. Nonoptimized bulk heterojunction solar cells, combining MDMO-PPV or MPE-PPV with [60]PCBM (1:4 ratio), were made with a general ITO/PEDOT−PSS/polymer:[60]PCBM/Ca/Al structure. Table 1 shows the initial values of short circuit current, fill factor, open circuit voltage, and the efficiency of the solar cells. The initial *IV* curves are depicted in Figure 4. The initial efficiencies were in the range of 1.3% for both PPV polymers. The MPE-PPV devices show similar V_{oc} and substantial higher I_{sc} than those based on MDMO-PPV, indicating potential for improved performance. These first devices were, however, not optimized for maximum performance.

When these solar cells are to be used outdoors in full sunlight, the devices must be able to withstand the temperatures as high as 75 °C reached in such case. Previous studies already demonstrated that the poor thermal stability of MDMO-PPV:[60]PCBM solar cells resulted in a gradual decrease of the efficiency upon heating.[22,23] The use of conjugated polymers with a T_g substantially above 75 °C as a donor material should render the amorphous polymer:fullerene phase glassy at this maximum operation temperature, drastically slowing down diffusion rates and basically preventing the further growth of the [60]PCBM crystals, thus overall resulting in a better thermal stability of the device. Hence, it is expected that, although the initial efficiency values are about the same for both devices, the MPE-PPV:[60]PCBM solar cells will have a better resistance toward high temperatures than MDMO-PPV:[60]PCBM-based solar cells.

To verify this hypothesis, both devices were annealed at two different temperatures, either 90 or 110 °C, in a dark nitrogen atmosphere for 100 h. In addition, the thermally more stable MPE-PPV:[60]PCBM solar cells were also annealed at an even higher temperature of 130 °C. These temperatures are all well-above the T_g of the MDMO-PPV:[60]PCBM (1:4) blend, while being below, near, and above the T_g of the MPE-PPV:[60]PCBM (1:4) blend. During the annealing treatment, the *IV* characteristics were monitored at specific time intervals. Figure 5 shows the relative decay of the photovoltaic parameters of both solar cells for the different annealing temperatures. In most cases the open circuit voltage (V_{oc}) is barely sensitive to the thermal treatment performed over a long period of time. Thermal annealing of the solar cells at all temperatures resulted in small decreases in V_{oc} of about 10−13% (Figure 5b and Table 1). This is consistent with the fact that the V_{oc} mainly depends on material properties, i.e., the ionization potential of the donor polymer and the electron affinity of the acceptor fullerene molecule. After 100 h the short circuit current of the MPE-PPV solar cells showed a decrease of 18% when annealed at 90 or 110 °C and a decrease of 29% when annealed at 130 °C. The MDMO-PPV-based solar cells suffered more substantially from the annealing process.

Table 1. Values of Short Circuit Current (I_{sc}), Open Circuit Voltage (V_{oc}), Fill Factor (FF), and Power Conversion Efficiency (η) for MPE-PPV:[60]PCBM and MDMO-PPV:[60]PCBM (1:4) Solar Cells, Spin-Coated from Chlorobenzene (Initial Values and Values after Thermal Annealing)

polymer:[60]PCBM (1:4)	annealing	I_{sc} (mA/cm^2)	V_{oc} (V)	FF	η (%)
MPE-PPV:[60]PCBM	0 h (25 °C)	4.14	0.783	0.40	1.30
	100 h at 90 °C	3.38	0.692	0.39	0.91
	100 h at 110 °C	3.39	0.733	0.35	0.88
	100 h at 130 °C	2.92	0.713	0.37	0.76
MDMO-PPV:[60]PCBM	0 h (25 °C)	2.87	0.785	0.60	1.30
	100 h at 90 °C	1.70	0.710	0.43	0.52
	100 h at 110 °C	1.45	0.685	0.42	0.40

Annealing at 90 °C resulted in a decrease of 41% of the initial short circuit current while annealing at 110 °C resulted in a decrease of 49%. After 100 h of annealing, the fill factor of the MPE-PPV solar cells showed small decreases between 2 and 12%. The fill factor of MDMO-PPV solar cells decreased 28−30%. Finally, after 100 h, the overall efficiency, being proportional to the short-circuit current and the fill factor, is much more stable for MPE-PPV-based solar cells (a decrease of 30% after annealing at 90 °C, a decrease of 32% after annealing at 110 °C, and a decrease of 42% after annealing at 130 °C) as compared to MDMO-PPV-based solar cells (a decrease of 61% after annealing at 90 °C and a decrease of 69% after annealing at 110 °C). These results are consistent with earlier reported observations on a commercial high-T_g PPV terpolymer.[22,23] The importance of the relative position of the glass transition of the conjugated polymer with respect to the temperature at which the performance stability is evaluated is clearly seen.

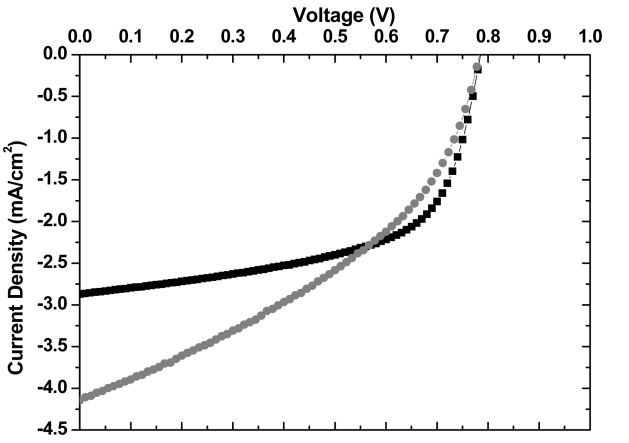

Figure 4. Current−voltage characteristics obtained for MPE-PPV:[60]PCBM (gray circles) and MDMO-PPV:[60]PCBM (black squares) (1:4) solar cells under AM 1.5 illumination.

The higher thermal stability of the MPE-PPV solar cells is revealed not only in the photovoltaic parameters but also in the bulk morphology of the active layer. The blend morphology of both types of solar cells was studied with TEM (Figure 6). For the MDMO-PPV:[60]PCBM blend, earlier TEM studies showed pronounced [60]PCBM cluster formation upon annealing at 110 °C.[22,23] After 2 h of annealing at 110 °C, all the [60]PCBM had diffused out of the blend. Figure 6 shows large [60]PCBM clusters (dark areas) formed very rapidly upon annealing at 130 °C.[19] The selected area electron diffraction (SAED) patterns (insets in Figure 6) indicated that the clusters were groups of single [60]PCBM crystals. After only 0.5 h of annealing at 130 °C, the homogeneous MDMO-PPV:[60]PCBM matrix disappeared. Most of the [60]PCBM had diffused out of the blend and assembled in the [60]PCBM clusters. The same process occurred upon annealing at 90 °C, only slower (see Supporting Information). After 20 h of annealing at 90 °C, [60]PCBM crystals were formed. Because of the smaller interfacial area between donor

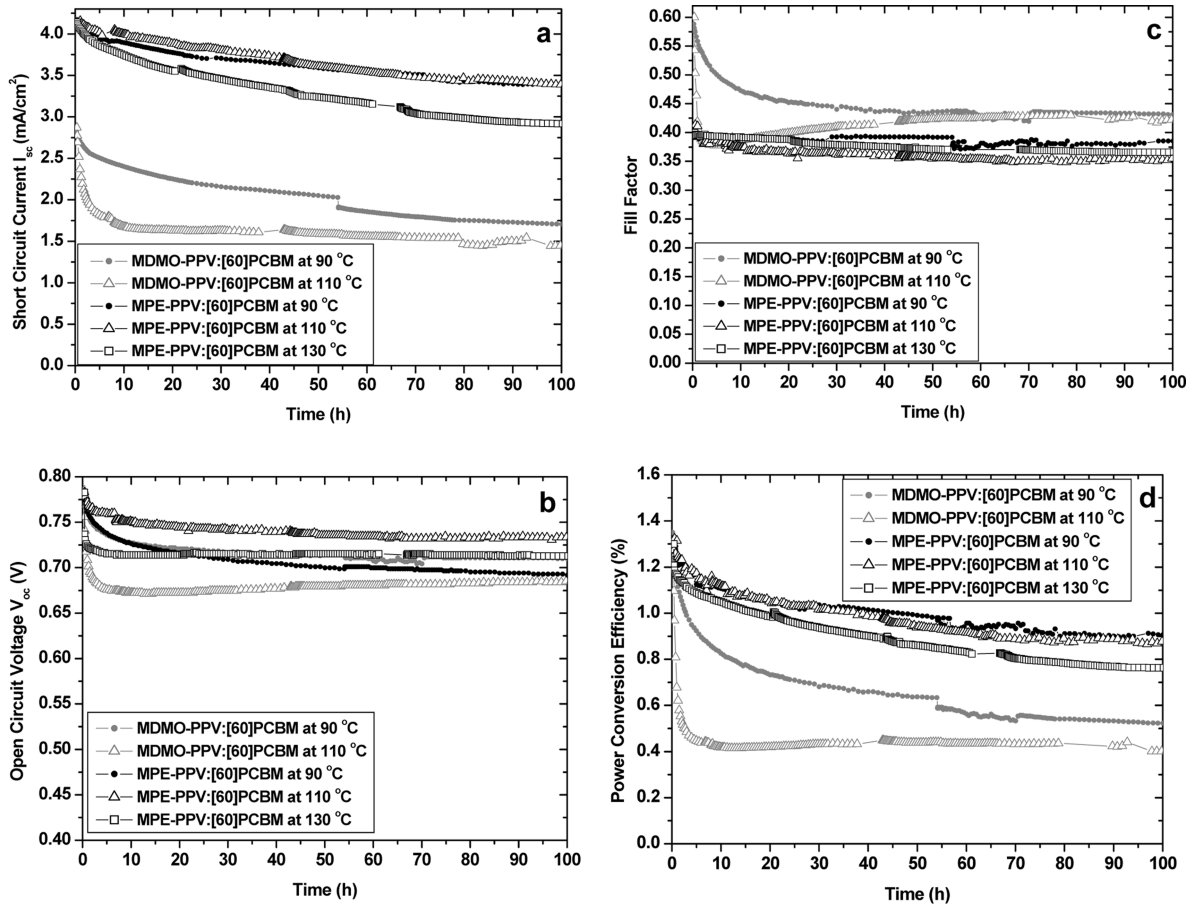

Figure 5. Relative decay of short circuit current I_{sc} (a), open circuit voltage V_{oc} (b), fill factor (c), and power conversion efficiency (d) for MDMO-PPV:[60]PCBM (1:4) solar cells (gray) and MPE-PPV:[60]PCBM (1:4) solar cells (black), during annealing at different temperatures.

dx.doi.org/10.1021/ma201911a |*Macromolecules* 2011, 44, 8470–8478

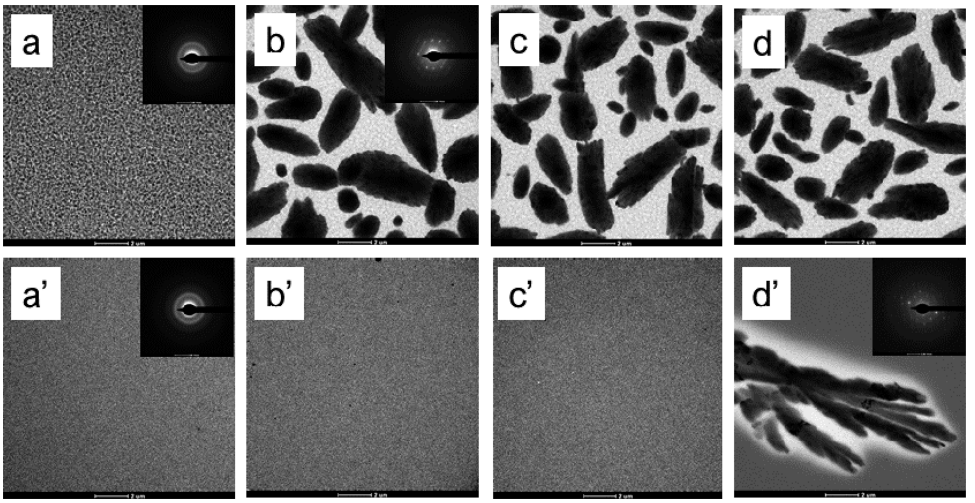

Figure 6. Bright-Field TEM images of the active layer of MDMO-PPV:[60]PCBM (1:4) solar cells (a−d) and MPE-PPV:[60]PCBM (1:4) solar cells (a′−d′), spin-coated from chlorobenzene, after annealing at 130 °C for 0 h (a, a′), 0.5 h (b, b′), 4 h (c, c′), and 20 h (d, d′) (scale bar: 2 μm). Insets: SAED patterns of matrix (a, a′) and [60]PCBM clusters (b, d′).

Table 2. Values of Short Circuit Current (I_{sc}), Open Circuit Voltage (V_{oc}), Fill Factor (FF), and Power Conversion Efficiency (η) for Different MPE-PPV:Fullerene (1:4) Solar Cells and a Reference MDMO-PPV:[70]PCBM (1:4) Solar Cell, Spin-Coated from Different Solvents, at Room Temperature[a]

polymer:fullerene (1:4)	processing solvent	I_{sc} (mA/cm^2)	V_{oc} (V)	FF	η (%)
MPE-PPV:[60]PCBM	chloroform	3.31	0.84	0.45	1.25
MPE-PPV:[60]PCBM	chlorobenzene	2.87	0.83	0.42	1.00
MPE-PPV:[60]PCBM	toluene	3.14	0.78	0.42	1.03
MPE-PPV:[70]PCBM	chloroform	5.66	0.85	0.48	2.31
MPE-PPV:[70]PCBM	chlorobenzene	5.36	0.85	0.48	2.19
MPE-PPV:[70]PCBM	toluene	4.87	0.80	0.47	1.83
MDMO-PPV:[70]PCBM	1,2-dichlorobenzene	6.52	0.80	0.57	2.97

[a] The currents reported are corrected for spectral mismatch.

and acceptor material, the photocurrent output decreased, as was demonstrated above. The TEM images of the active layer of the MPE-PPV solar cells (Figure 6a′−d′) showed a much more stable morphology. The film had to be annealed for 20 h at the highest temperature of 130 °C before a [60]PCBM cluster was detected. Because of the considerably lower T_g (45 °C) of MDMO-PPV, the [60]PCBM is able to crystallize at a higher rate in MDMO-PPV:[60]PCBM active layers than in high-T_g MPE-PPV:-[60]PCBM active layers. When the solar cell is subjected to temperatures below the T_g of the applied polymer, the matrix is in a glassy state and the fullerene molecules are restricted to move freely. Thermal treatments near or above T_g cause the matrix to devitrify and rendering it much easier for the fullerene molecules to move and cluster.

As can be observed from the TEM images, the MPE-PPV:-[60]PCBM solar cells do not exhibit an initial fine nanoscale phase separation, as compared to MDMO-PPV:[60]PCBM solar cells, in agreement with the single T_g observed for the MPE-PPV:[60]PCBM. This correlates also with the quite low fill factor of the obtained MPE-PPV based devices (FF = 0.40) compared to MDMO-PPV based solar cells (FF = 0.60). To improve this initial morphology, an optimization study was performed whereby the active layers were spin-coated from either chloroform, chlorobenzene, or toluene. Because of the varying solubility characteristics of both the polymer and fullerene materials in the different solvents, the initial morphology of the active layer will be influenced to a large extent. In addition, not only [60]PCBM was used as an electron acceptor but also the [70]PCBM derivative, which in some solvents can crystallize more easily than [60]PCBM.[37] The results are shown in Table 2 and Figure 7.

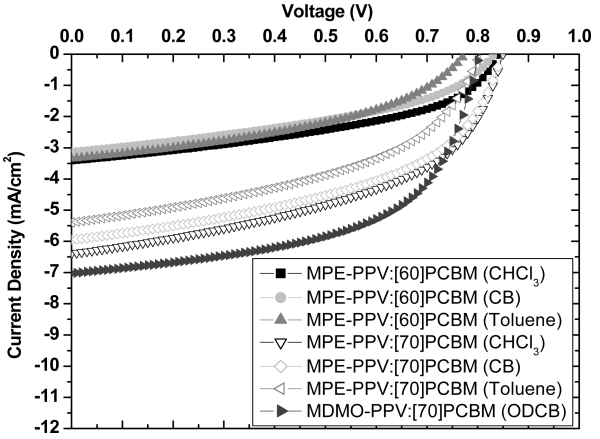

Figure 7. Current−voltage characteristics obtained for differentMPE-PPV:fullerene (1:4) solar cells and a reference MDMO-PPV:[70]PCBM (1:4) solar cell under AM 1.5 illumination (not corrected for spectral mismatch).

From the *IV* data, it can be derived that the use of [70]PCBM as the acceptor resulted in a substantial improvement of the device performance, mainly due to an improved light absorption of [70]PCBM, compared to [60]PCBM.[38] Consequently, higher current densities in the corresponding photovoltaic cells were observed. This was already demonstrated previously for MDMO-PPV:[70]PCBM solar cells, for which 1,2-dichlorobenzene proved to be the best processing solvent.[37] The *IV* characteristics have been added to Table 2 for comparison. Furthermore, the fill factor of MPE-PPV:[70]PCBM solar cells could be increased to 0.48, indicating an improved initial nanoscale phase-separated morphology. Chloroform was found to be the best processing solvent for MPE-PPV:fullerene solar cells, and the most efficient device displayed an efficiency of 2.3%, after correction for spectral mismatch.[8] The investigation of the thermal stability of this optimized MPE-PPV:[70]PCBM solar cell and the comparison with the results obtained for the initial MPE-PPV:[60]PCBM devices will be the subject of a follow-up study.

CONCLUSIONS

A novel PPV polymer, poly[2-methoxy-5-(2′-phenylethoxy)-1,4-phenylenevinylene] (MPE-PPV), with a T_g of 111 °C, has been synthesized by an efficient three-step Gilch protocol and has been explored as donor material in bulk heterojunction solar cells, demonstrating at the same time the engineering of T_g by stiffening the side-chain structure. The thermal stabilities of the nanomorphology of MDMO-PPV:fullerene and MPE-PPV:fullerene blends were compared, and the solar cell efficiencies of devices made from these blends were analyzed. Using [70]PCBM instead of [60]PCBM as acceptor resulted in a 70% increase in current density and device efficiency, with an optimized MPE-PPV:[70]PCBM device efficiency of 2.3%. It can be concluded that devices based on high-T_g MPE-PPV clearly outperform the MDMO-PPV:[60]PCBM-based solar cells in terms of a (thermally) more stable bulk (nano)morphology and a longer lifetime. For the MPE-PPV:[60]PCBM active layer, the high-T_g polymer matrix reduces the diffusion of the fullerene molecules, thereby slowing down the detrimental clustering process and maintaining a large interfacial area between donor and acceptor. It has hence been shown that the use of a high-T_g polymer is an effective way toward the development of more stable and efficient organic photovoltaic devices.

ASSOCIATED CONTENT

Supporting Information. Bright-field TEM images of the active layer of MDMO-PPV:[60]PCBM 1:4 solar cells and MPE-PPV:[60]PCBM 1:4 solar cells, spin-coated from chlorobenzene, after annealing at 90 °C for 0, 0.5, 4, and 20 h. This material is available free of charge via the Internet at http://pubs.acs.org.

AUTHOR INFORMATION

Corresponding Author

*Phone: +32 (0)11 26 83 21. Fax: +32 (0)11 26 83 01. E-mail: dirk.vanderzande@uhasselt.be.

ACKNOWLEDGMENT

The authors gratefully acknowledge the Fund for Scientific Research-Flanders (FWO) (PhD grants for J.V. and S.B., the project G.0091.07, postdoctoral grant for W.M.) and the Belgian Science Policy (BELSPO) in the frame of network IAP P6/27, initiated by the Belgian State Prime Minister's Office, for their financial support. We also thank the Institute for the Promotion of Innovation by Science and Technology in Flanders (IWT) for the financial support via the IWT-SBO project 060843 "Polyspec". TA Instruments is acknowledged for support through "Project RHC". We also thank F. Piersimoni and J. D'Haen for help with the experimental setup.

REFERENCES

(1) Brabec, C. J.; Gowrisanker, S.; Halls, J. J. M.; Laird, D.; Jia, S.; Williams, S. P. *Adv. Mater.* **2010**, *22*, 3839–3856.
(2) Moulé, A. J.; Meerholz, K. *Adv. Funct. Mater.* **2009**, *19*, 3028–3036.
(3) Shaheen, S. E.; Brabec, C. J.; Sariciftci, N. S.; Padinger, F.; Fromherz, T.; Hummelen, J. C. *Appl. Phys. Lett.* **2001**, *78*, 841–843.
(4) Munters, T.; Martens, T.; Goris, L.; Vrindts, V.; Manca, J.; Lutsen, L.; De Ceuninck, W.; Vanderzande, D.; De Schepper, L.; Gelan, J.; Sariciftci, N. S.; Brabec, C. J. *Thin Solid Films* **2002**, *403*−*404*, 247–251.
(5) Ma, W.; Yang, C.; Gong, X.; Lee, K.; Heeger, A. J. *Adv. Funct. Mater.* **2005**, *15*, 1617–1622.
(6) Padinger, F.; Fromherz, T.; Denk, P.; Brabec, C. J.; Zettner, J.; Hierl, T.; Sariciftci, N. S. *Synth. Met.* **2001**, *121*, 1605–1606.
(7) During final redaction of this manuscript, a special issue appeared on the 3th International Summit on OPV Stability: Krebs, F. C., Ed. *Sol. Energy Mater. Sol. Cells* **2011**, *95*, 1251−1418.
(8) Kroon, J. M.; Wienk, M. M.; Verhees, W. J. H.; Hummelen, J. C. *Thin Solid Films* **2002**, *403*−*404*, 223–228.
(9) Krebs, F. C.; Carlé, J. E.; Cruys-Bagger, N.; Andersen, M.; Lilliedal, M. R.; Hammond, M. A.; Hvidt, S. *Sol. Energy Mater. Sol. Cells* **2005**, *86*, 499–516.
(10) Schuller, S.; Schilinsky, P.; Hauch, J.; Brabec, C. J. *Appl. Phys. A: Mater. Sci. Process.* **2004**, *79*, 37–40.
(11) Neugebauer, H.; Brabec, C.; Hummelen, J. C.; Sariciftci, N. S. *Sol. Energy Mater. Sol. Cells* **2000**, *61*, 35–42.
(12) Camaioni, N.; Ridolfi, G.; Casalbore-Miceli, G.; Possamai, G.; Garlaschelli, L.; Maggini, M. *Sol. Energy Mater. Sol. Cells* **2003**, *76*, 107–113.
(13) Hoppe, H.; Sariciftci, N. S. *J. Mater. Res.* **2004**, *19*, 1924–1945.
(14) Neugebauer, H.; Brabec, C. J.; Hummelen, J. C.; Janssen, R. A. J.; Sariciftci, N. S. *Synth. Met.* **1999**, *102*, 1002–1003.
(15) Krebs, F. C.; Spanggaard, H. *Chem. Mater.* **2005**, *17*, 5235–5237.
(16) Krebs, F. C.; Norrman, K. *Prog. Photovoltaics* **2007**, *15*, 697–712.
(17) Conings, B.; Bertho, S.; Vandewal, K.; Senes, A.; D'Haen, J.; Manca, J.; Janssen, R. A. J. *Appl. Phys. Lett.* **2010**, *96*, 163301.
(18) Yang, X.; van Duren, J. K. J.; Rispens, M. R.; Hummelen, J. C.; Janssen, R. A. J.; Michels, M. A. J.; Loos, J. *Adv. Mater.* **2004**, *16*, 802–806.
(19) Yang, X.; van Duren, J. K. J.; Janssen, R. A. J.; Michels, M. A. J.; Loos, J. *Macromolecules* **2004**, *37*, 2151–2158.
(20) Yang, X.; Loos, J.; Veenstra, S. C.; Verhees, W. J. H.; Wienk, M.; Kroon, J. M.; Michels, M. A. J.; Janssen, R. A. J. *Nano Lett.* **2005**, *5*, 579–583.
(21) Campo, B.; Oosterbaan, W.; Gilot, J.; Cleij, T.; Lutsen, L.; Janssen, R. A. J.; Vanderzande, D. *Proc. SPIE* **2009**, *7416*, 74161G.
(22) Bertho, S.; Haeldermans, I.; Swinnen, A.; Moons, W.; Martens, T.; Lutsen, L.; Vanderzande, D.; Manca, J.; Senes, A.; Bonfiglio, A. *Sol. Energy Mater. Sol. Cells* **2007**, *91*, 385–389.
(23) Bertho, S.; Janssen, G.; Cleij, T. J.; Conings, B.; Moons, W.; Gadisa, A.; D'Haen, J.; Goovaerts, E.; Lutsen, L.; Manca, J.; Vanderzande, D. *Sol. Energy Mater. Sol. Cells* **2008**, *92*, 753–760.
(24) Deimede, V.; Kallitsis, J. K.; Pakula, T. *J. Polym. Sci., Part A: Polym. Chem.* **2001**, *39*, 3168–3179.
(25) Strukelj, M.; Papadimitrakopoulos, F.; Miller, T. M.; Rothberg, L. J. *Science* **1995**, *267*, 1969–1972.
(26) Johansson, D. M.; Srdanov, G.; Yu, G.; Theander, M.; Inganas, O.; Andersson, R. M. *Macromolecules* **2000**, *33*, 2525–2529.
(27) Gilch, H. G.; Wheelwright, W. L. *J. Polym. Sci.* **1966**, *4*, 1337–1349.

(28) Thompson, B. C.; Fréchet, J. M. J. *Angew. Chem., Int. Ed.* **2008**, *47*, 58–77.
(29) Yang, X.; Loos, J. *Macromolecules* **2007**, *40*, 1353–1362.
(30) Moulé, A. J.; Meerholz, K. *Adv. Mater.* **2008**, *20*, 240–245.
(31) Mueller, C.; Ferenczi, T. A. M.; Campoy-Quiles, M.; Frost, J. M.; Bradley, D. D. C.; Smith, P.; Stingelin-Stutzmann, N.; Nelson, J. *Adv. Mater.* **2008**, *20*, 3510–3515.
(32) Kim, J. Y.; Frisbie, C. D. *J. Phys. Chem. C* **2008**, *112*, 17726–17736.
(33) Zhao, J.; Swinnen, A.; Van Assche, G.; Manca, J.; Vanderzande, D.; Van Mele, B. *J. Phys. Chem. B* **2009**, *113*, 1587–1591.
(34) Danley, R. L.; Caulfield, P. A.; Aubuchon, S. R. *Am. Lab.* **2008**, *40*, 9–11.
(35) Miltner, H. E.; Grossiord, N.; Lu, K.; Loos, J.; Koning, C. E.; Van Mele, B. *Macromolecules* **2008**, *41*, 5753–5762.
(36) Zhao, J.; Bertho, S.; Vandenbergh, J.; Van Assche, G.; Manca, J.; Vanderzande, D.; Cleij, T.; Lutsen, L.; Van Mele, B. *Phys. Chem. Chem. Phys.* **2011**, *13*, 12285–12292.
(37) Wienk, M. M.; Kroon, J. M.; Verhees, W. J. H.; Knol, J.; Hummelen, J. C.; van Hal, P. A.; Janssen, R. A. J. *Angew. Chem., Int. Ed.* **2003**, *42*, 3371–3375.
(38) Arbogast, J. W.; Foote, C. S. *J. Am. Chem. Soc.* **1991**, *113*, 8886–8889.